

Article

Street Design Strategies Based on Spatial Configurations and Building External Envelopes in Relation to Outdoor Thermal Comfort in Arid Climates

Fatima Zahra Ben Ratmia ^{1,2}, Atef Ahriz ^{3,4} , Giovanni Santi ⁵ , Soumia Bouzaher ², Waqas Ahmed Mahar ^{6,7} , Mohamed Akram Eddine Ben Ratmia ² and Mohamed Elhadi Matallah ^{1,2,7,*} 

- ¹ Laboratory of Design and Modeling of Architectural and Urban Forms and Ambiances (LACOMOFA), Mohamed Khider University, Biskra 07000, Algeria; fatimazahra.benratmia@univ-biskra.dz
 - ² Department of Architecture, Mohamed Khider University, Biskra 07000, Algeria; s.bouzaherlalouani@univ-biskra.dz (S.B.); akrameddine.benratmia@univ-biskra.dz (M.A.E.B.R.)
 - ³ Department of Architecture, Echahid Cheikh Larbi Tebessi University, Tebessa 12000, Algeria
 - ⁴ Laboratory of Applied Civil Engineering (LGCA), Echahid Cheikh Larbi Tebessi University, Tebessa 12000, Algeria
 - ⁵ Department of Energy, Systems, Territory and Construction Engineering, University of Pisa, 56122 Pisa, Italy; giovanni.santi@unipi.it
 - ⁶ Faculty of Architecture and Town Planning (FATP), Aror University of Art, Architecture, Design and Heritage, Sukkur 65200, Pakistan; waqas.faculty@aror.edu.pk
 - ⁷ Sustainable Building Design (SBD) Lab, Department of Urban and Environmental Engineering (UEE), Faculty of Applied Sciences, Université de Liège, 4000 Liège, Belgium
- * Correspondence: elhadi.matallah@univ-biskra.dz

Abstract: Climate change patterns and expected extreme weather conditions drive urban design practices toward more effective adaptation strategies for the built environment. Biskra City, one of the largest urban areas in the Algerian Sahara territory, has suffered from unprecedented extreme weather patterns, specifically during the summer. This paper examined outdoor thermal comfort in the arid climates of Biskra, Algeria, during summer extreme conditions by investigating the impact of the height-to-width (H/W) ratio aspect and the north–south (N-S) and east–west (E-W) street orientations on pedestrian thermal comfort with the parameterization of external building envelopes using brick, concrete, adobe, and limestone materials. This study was conducted with ENVI-met 5.1.1 software, based on 24 parametric scenarios, to identify the most effective composition for outdoor thermal stress mitigation using the physiological equivalent temperature (PET) thermal index. Across all scenarios, the PET index values fluctuated between PET_{min} = 32.2 °C and PET_{max} = 60.6 °C at different hours. The coupling between the H/W ratio and street orientation as geometry factors and building envelope characteristics reveals six distinct categories of building materials, each with an impact on outdoor thermal comfort: (1) high cooling (60–100%), (2) medium cooling (40–60%), (3) low cooling (<40%), (4) high heating (60–100%), (5) medium heating (40–60%), and (6) low heating material (<40%). Therefore, in the N-S orientation, limestone walls can provide a cooling efficiency range from 85% to 100% throughout deep and shallow canyons. Contrary to this, brick walls can cause a heat retention range varying from 70% to 93% within the same canyons. When considering extreme summer conditions in arid climates, the results show that the most effective bioclimatic passive strategy that could be achieved is the E-W orientation, within H/W < 1, characterized by a high albedo building material.

Keywords: heat stress; BWh; street canyon; physiological equivalent temperature; ENVI-met; parameterization



Citation: Ben Ratmia, F.Z.; Ahriz, A.; Santi, G.; Bouzaher, S.; Mahar, W.A.; Ben Ratmia, M.A.E.; Matallah, M.E. Street Design Strategies Based on Spatial Configurations and Building External Envelopes in Relation to Outdoor Thermal Comfort in Arid Climates. *Sustainability* **2024**, *16*, 221. <https://doi.org/10.3390/su16010221>

Academic Editor: Fausto Cavallaro

Received: 16 November 2023

Revised: 17 December 2023

Accepted: 20 December 2023

Published: 26 December 2023



Copyright: © 2023 by the authors. Licensee MDPI, Basel, Switzerland. This article is an open access article distributed under the terms and conditions of the Creative Commons Attribution (CC BY) license (<https://creativecommons.org/licenses/by/4.0/>).

1. Introduction

In the present day, rapid urbanization underscores the urgent necessity to build suitable living environments, infrastructures, and various facilities to meet the essential

requirements of the growing population. Faced with global warming, the human comfort thresholds inside urban areas have become increasingly vulnerable, leading to various health issues, such as cardiovascular diseases with heat stroke and cardiorespiratory diseases [1,2]. Additionally, there has been a significant surge in energy consumption for cooling purposes [3,4]. In this context, there is a compelling demand for more effective and adaptive urban planning and development practices to enhance quality of life.

Several studies have started to explore the impact of urban fabrics with their building materials characteristics on outdoor human thermal comfort and urban heat island (UHI) effects [5–12]. Additionally, many previous studies have also focused on a one-factor group to evaluate the thermal comfort levels within different scales without investigating a combination of factors, particularly with building material characteristics. In this regard, the elaboration of urban design strategies related to outdoor thermal comfort has been conducted in diverse contexts and under various approaches. In a study by Deng and Wong [13], conducted in 2020, the researchers investigated the impact of the H/W aspect ratio, the sky view factor (SVF), and urban canyon orientation as critical street geometry factors influencing microclimate variables at the pedestrian levels in Nanjing, China. Their results revealed that outdoor thermal comfort is significantly driven by solar access, which is determined by the canyon aspect ratio and orientation. In a different context, the research conducted by Johansson [14] in Fez, Morocco, in 2006 was in a hot dry climate. The study concluded that a climate-conscious urban design should incorporate a compact urban form and deep street canyons to enhance outdoor thermal comfort. However, cities with cold winters in the same climates should include wider streets for greater solar access. Furthermore, in research by Ali-Toudert and Mayer conducted in 2006 [15], in the similar climate of Ghardaïa, Algeria, observed that the duration of high thermal stress within a street canyon strongly depends on its aspect ratio and street orientation. A study in tropical climates (Muniz-Gaal et al., 2020) [16] found that canyons with a higher H/W aspect ratio increase wind speed and shading by buildings, consequently improving thermal comfort at the pedestrian level, especially during the summer.

To the best of our knowledge, the combination of street geometry aspects and building envelopes for outdoor thermal comfort is very limited. Studies by Ali-Toudert, 2021 [6], Wonorahardjo et al., 2020 [17], Rosso et al., 2018 [18], and Schrijvers et al., 2017 [19] explored the impact of street canyons linked with the building materials of external walls on the outdoor thermal environment. As their main results, Ali-Toudert, 2021 [6] found that differences in heat stress magnitudes depend on the aspect ratio due to different road and wall fractions. On the other hand, thermal inertia and thermal insulation lead to different shares of sensible versus storage heat during the day. Wonorahardjo et al., 2020 [17] referred to high-density walls, such as those of brick and concrete storing heat, as causing a significant increase in heat island intensity (HII) during the afternoon hours. Rosso et al., 2018 [18] showed that cool materials can improve the microclimate without neglecting preservation constraints. These materials set the best thermal comfort scenarios by enhancing albedo on urban canyon surfaces. However, their application on the vertical surfaces of deep canyons can lead to increased effects of thermal discomfort. Moreover, in 2017, Schrijvers et al. [19] found that the most effective strategy to minimize thermal stress inside urban canyons with an aspect ratio $H/W = 0.5$ is a uniform albedo of 0.2. For $H/W = 1$, an albedo gradient from high at the bottom part to low at the top of the vertical walls of building envelopes showed the lowest thermal stress.

In this regard, this paper aims to investigate the impact of the coupling between street canyon spatial configuration and external building envelopes on outdoor thermal comfort. The focus is on determining adaptive urban design outlines specifically for arid climates, fostering a sustainable built environment over the long term. Therefore, it is crucial to ensure the sustainability of the vulnerable Saharan urban ecosystem for the benefit of future generations.

Consequently, this research is conducted in Biskra City, southern Algeria, which is one of the largest arid regions of North Africa. Biskra City is currently undergoing a

remarkable change in its microclimate, particularly during the summer season. Therefore, the succession of heat waves causes extreme heat stress and limits human activities for extended periods.

In this regard, this study relies mainly on an empirical approach and numerical modeling based on continuous field measurements, in which the research outcomes can be applied to large arid cities worldwide, specifically in North African arid lands. The emphasis is based on street geometry and external building materials parametrization. Two research questions were asked to address the problem of this study:

- (1) How do variations in the H/W aspect ratio, street canyon orientation, and building external materials interact to impact outdoor thermal comfort at different levels in arid climates?
- (2) What spatial configurations and parametric details should be considered to achieve appropriate thermal comfort ranges within urban canyons?

To answer the research questions, this paper demonstrates 24 designed scenarios that combined H/W aspect ratios, canyons orientations, and external building materials concerning outdoor thermal comfort using the physiological equivalent temperature (PET) index [20–23] and supported with numerical modeling and simulations using CFD ENVI-met 5.1.1 software [24,25]. This paper's originality lies in determining urban design practices related to various canyons' geometries, orientations, and external envelopes to effectively adapt to extreme weather conditions in arid environments. The findings of this study show that urban guidelines can be readily applied to enhance walkability [26–28] and meet outdoor activity requirements during the summer period.

2. Materials and Methods

The current study used three methods: field measurements, numerical modeling, and simulations. We followed an empirical approach to determine urban design guidelines that couple urban canyon geometry with a building's external envelope in relation to human outdoor thermal comfort. Figure 1 illustrates this study's conceptual framework, outlining the main steps from site data collection to numerical modeling and simulation data processing. The following subsections provide a detailed explanation of the research methodology.

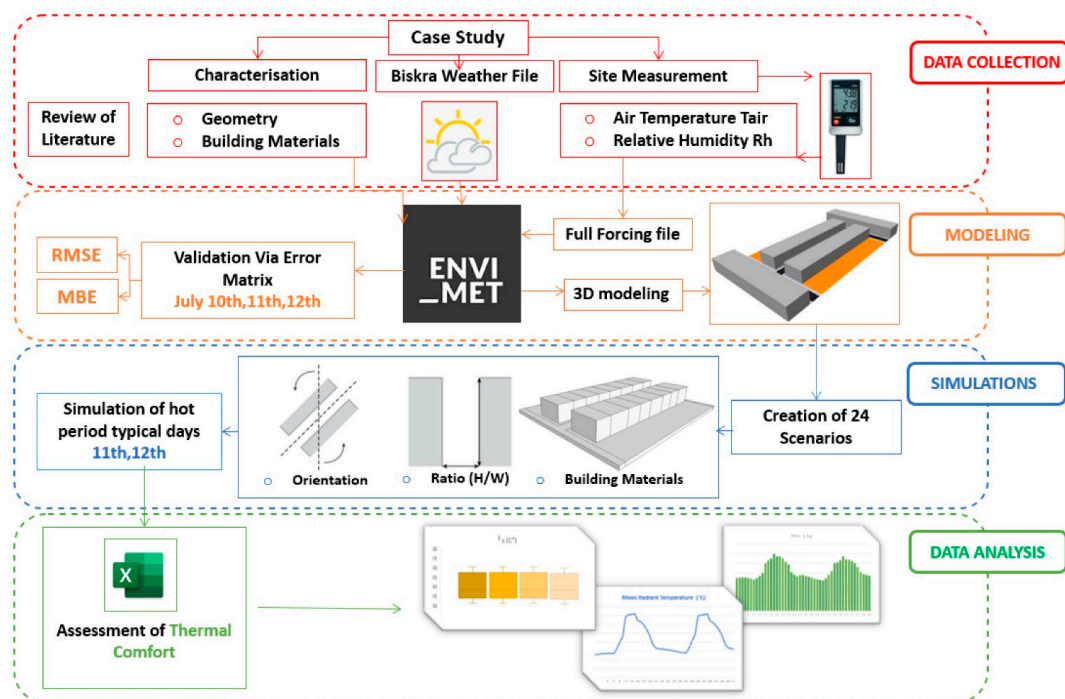


Figure 1. The conceptual framework of this study.

2.1. Site Fields

This study was conducted in Biskra City, the capital of the ‘Ziban’ region, one of the largest oasis territories in the southeast of Algeria. The region is named the ‘Gateway of Sahara’ due to its location at the northern frontier of the Algerian Sahara and takes the name of Biskra as the largest city [29,30]. The city is situated at a latitude of 34.793 north and a longitude of 5.738 east and has an elevation of 88 m above sea level, as shown in Figure 2. As of 2022, Biskra City had 730,000 inhabitants, making it the region’s most densely populated city. The territory is known for date palm cultivation, with over 4,000,000 million palm trees implantations of diverse varieties, most notably, the worldwide high-quality ‘Deglet Nour’ variety [31]. The Ziban region is considered the primary agricultural pivot in local food exchanges and one of the favorable export resources contributing to the Algerian economy [32].

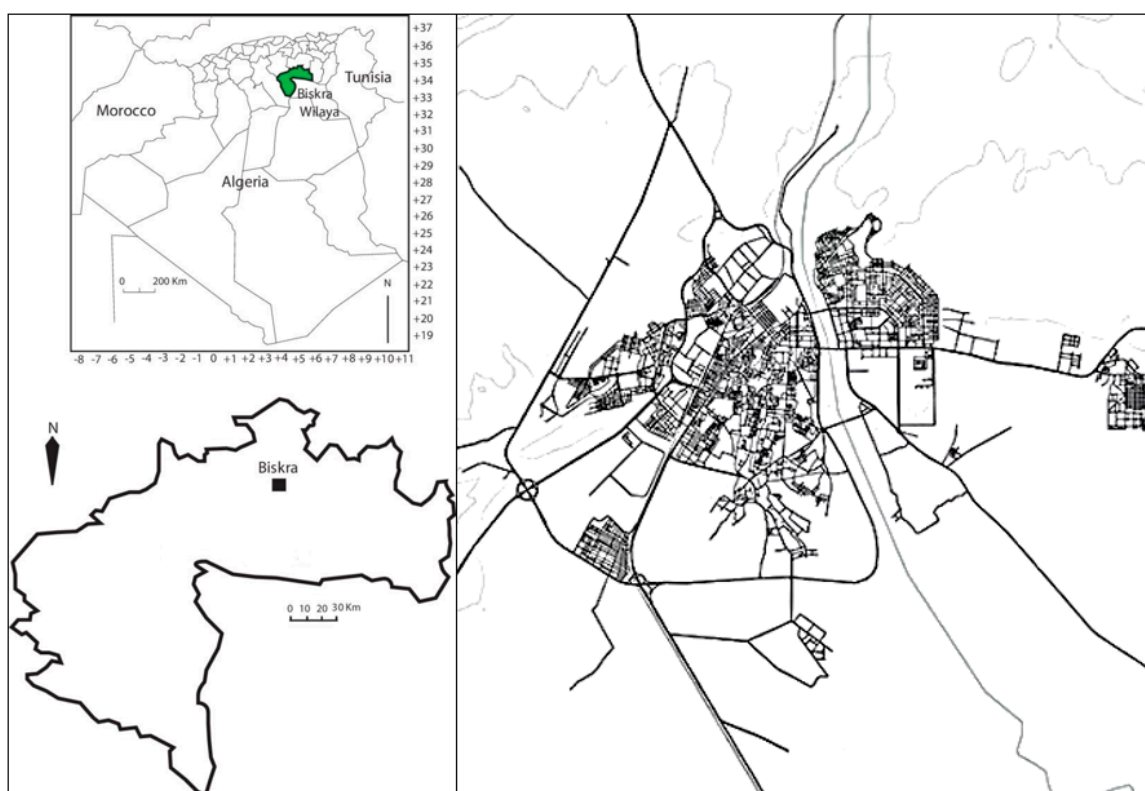


Figure 2. Location of Biskra City in the territory of the country.

According to the Koppen–Geiger classification, the region’s climate is classified as a hot and dry climate (BWh). Therefore, between 1958 and 2021, the yearly recorded average air temperature was 22.4 °C, with a maximum value of 41.9 °C versus a minimum value of 6.4 °C (Figure 3) (Center for the Built Environment (CBE), 2021) [33]. July is the hottest month, with maximum temperatures reaching 45 °C. Conversely, January is the coldest period, with minimum temperatures equal to 1 °C. The average relative humidity is consistently low, hovering around 47%, with a maximum value of 65% recorded in December and a minimum of 28.3% in July and August.

Rainfall in the Ziban region is characterized by irregularity and scarcity, with an annual average of 126 mm. During the last decade, the region has endured extended periods of drought, sometimes lasting throughout the year.

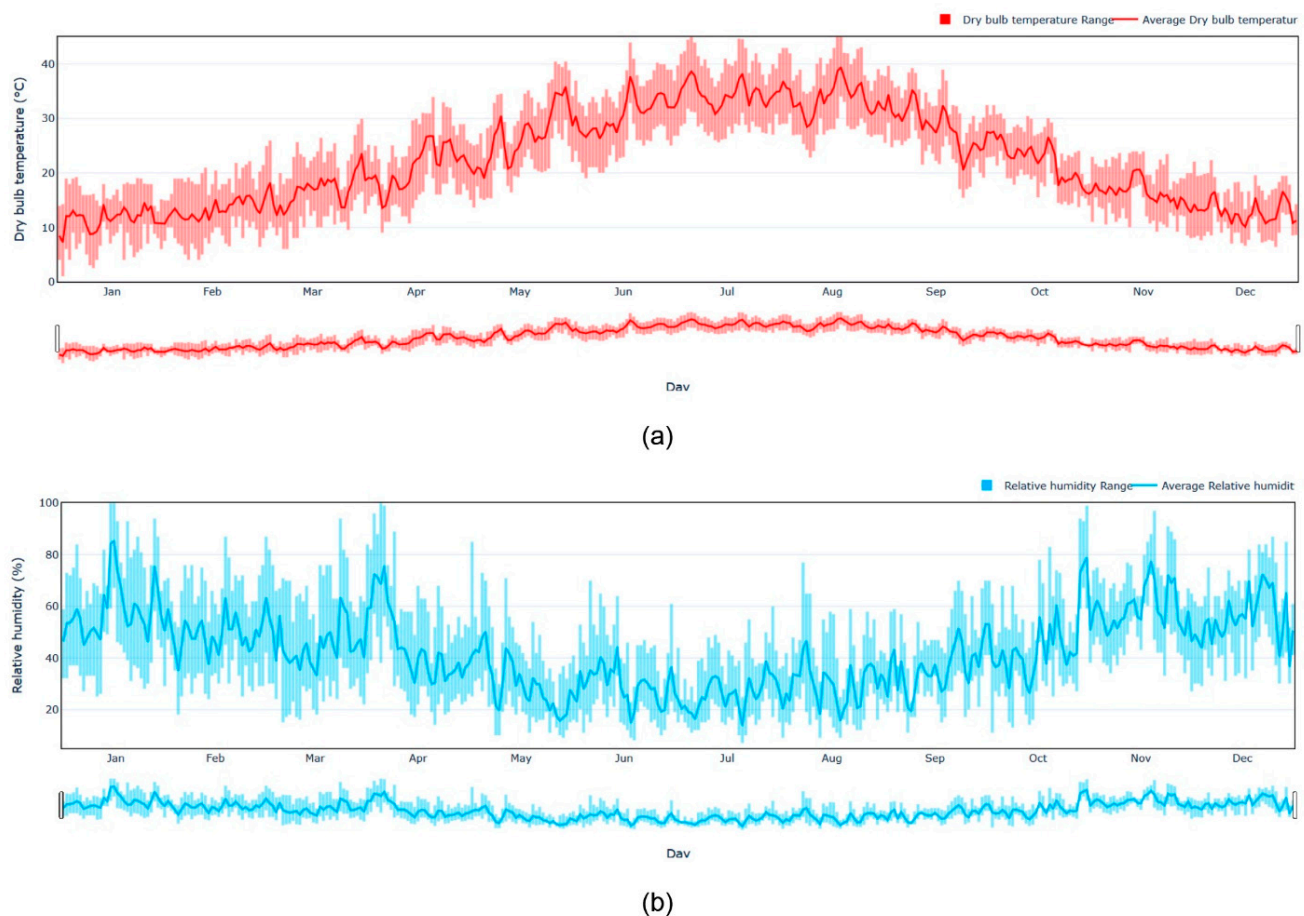


Figure 3. Climatic conditions of this study's context: (a) dry bulb temperature and (b) relative humidity, exported from the CBE website [33].

Characterization of the Biskra City Housing Sector

Biskra holds a significant strategic position and is also known as a gateway to the Algerian Sahara due to its vital geographical location. Therefore, it has been home to many civilizations. The city of Biskra has evolved through four main vital periods: the pre-colonial (Ottoman) period and the colonial, post-colonial, and contemporary periods [34]. These transformations have brought about crucial urban changes over centuries, affecting all aspects of its development, including different urban fabrics and housing typologies over centuries (Figure 4) [34].

The housing typology in Biskra presents several forms that differ from one neighborhood to another. Generally, Biskra housing comprises two main typologies: individual and collective multi-family housing [35]. Therefore, Figure 5, which presents a city building block, shows that the new individual block is the dominant type within the city with a rate of 76% versus 11% of the collective and semi-collective multi-family housing and the individual traditional housing, respectively, followed by only 2% of precarious individual housing. It is further divided into rural and self-constructed housing throughout the city borders.

The city's varied history offers a unique context with contrasting urban characteristics, including both old oasis settlements and new urban fabrics. The influence of culture and adaptation to the local environment has resulted in a wide diversity of building materials, blending traditional and modern construction materials. The old oasis settlement, which presented the first urban core within the palm groves south of the current city (Figure 4), was built using traditional local materials and methods, such as mud adobe, palm wood, and stone [36].

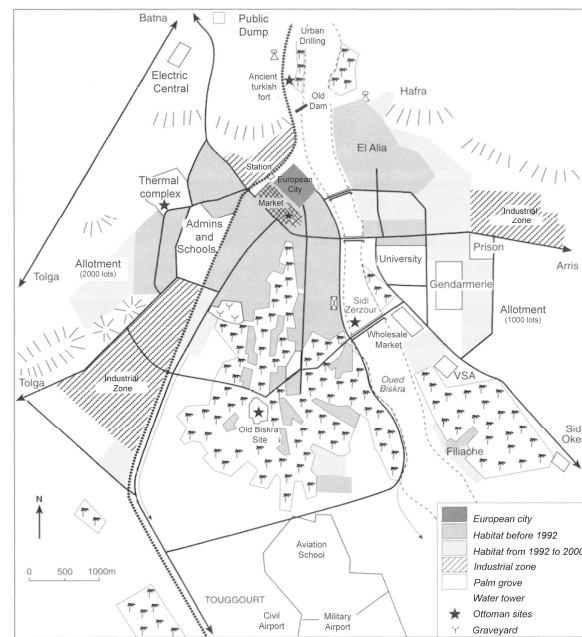


Figure 4. Old and new urban fabrics of Biskra City, adapted by the authors.

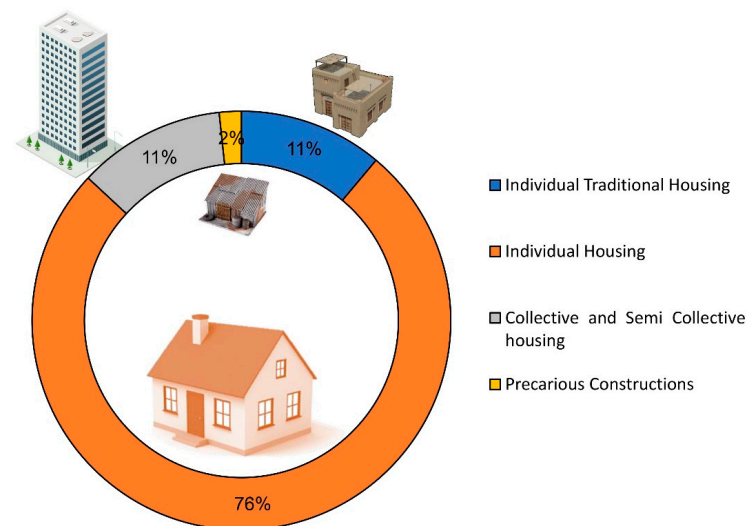


Figure 5. Housing typology in Biskra City (Algerian National Statistics Office, 2018).

On the other hand, new urban fabrics use modern building materials that correspond to contemporary construction needs, including concrete, steel, glass, and hollow brick.

2.2. Site and Sample Selection Criteria

The selected urban canyon of this study is located within an individual housing neighborhood in the southeast of the city of Biskra. The canyon's length is around 90 m, with a mean building height of 10 m.

The canyon has an aspect ratio of $H/W = 1$ and is oriented along the east–west direction (Figure 6). All the external walls are summed to have 30 cm thick walls made with hollow brick laid with a 20 mm layer of plaster and finished with a 30 mm layer of mortar.

The study area selection is mainly related to the characteristics of the most common housing types in Biskra City. These criteria are housing type, building materials, street aspect ratio, and orientation.



Figure 6. The location of the site in Biskra City.

2.3. In Situ Measurement

The current study uses hourly continuous measurements within the selected canyon between 10 April and 25 November 2021 to characterize the effect of the thermal behavior of external walls during a long period (Figure 7). This time frame represents the heat stress period, particularly during the summer season within this study's context. Table 1 reveals the monitoring data logger Testo 175 H1 characteristics that measure the air temperature (T_a) and relative humidity (R_H). The data logger's memory capacity was sufficient for one million data points when the recording was configured at 10-minute intervals. To manage the recorded datasets, it was essential to utilize the complementary numerical tool 'Comfort Software Basic'. It is necessary to indicate that the data logger was installed 30 cm away from a building's external wall, at a height of 1.4 m from the ground, to avoid any heat exchange from external lighting during the night or humidity generated by the nearby trees and grass. Harrison, 2014, has further discussed the measurement and data logger installation protocols [37].

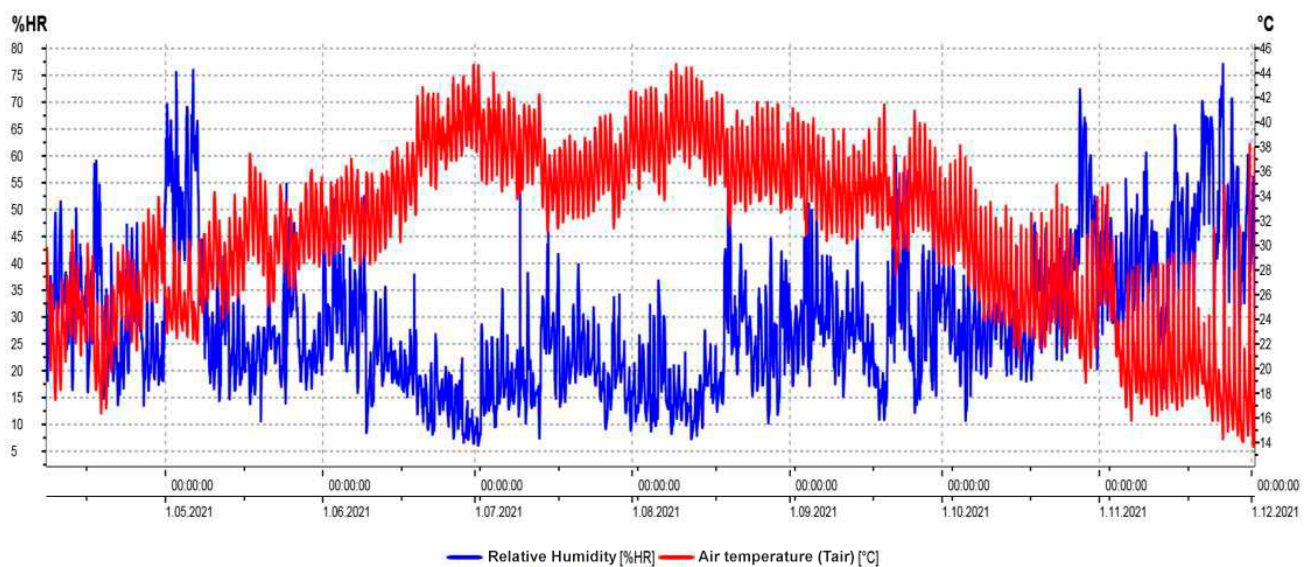


Figure 7. The field measurements of air temperature (T_a) and relative humidity (R_H).

Table 1. The details of the monitoring device used for this study.

Variable	Device	Dimensions	Unit	Accuracy	Range
Air temperature (Ta)	Testo 175 H1	149 × 53 × 27 mm	°C	±0.4 °C	−20 to + 55 °C
Relative humidity (RH)	0572 1754		%	±1.0%	0 to 100%

2.4. Model Creation and Simulation

The numerical models, named scenarios, were designed using the latest version of CFD ENVI-met software [24]. These scenarios encompass a range of various parameters, including the built environment and microclimatic conditions. The modeling encompasses 24 distinct scenarios, mainly focusing on the characteristics of building materials such as external walls, soils, and pavements.

Most studies use the ENVI-met software suite to assess the impacts of various urban geometries on outdoor thermal comfort and to predict the thermal effects of different mitigation scenarios [38,39]. ENVI-met is a prognostic, three-dimensional, grid-based microclimate model designed to simulate complex surface–vegetation–air interactions in the urban environment [40]. Thus, the software provides many tools to simulate and analyze an area’s microclimate and thermal comfort.

The initial scenario modeled is the baseline model, which serves as a reference for the study area. The baseline scenario ensures that all forms of the current urban geometry and building material characteristics specific to the study area are precisely represented. The streets’ initial orientation is east–west, while the walls and external pavements consist of brick, asphalt, and concrete.

Table 2 provides an overview of the building materials utilized in this study, which comprise several layers and different thermo-physical characteristics such as thermal conductivity, specific heat capacity, emissivity albedo, etc. All the building materials used in this study adhere to the Algerian thermal guidelines of the Algerian Centre for Building Integrated Studies and Research (CNERIB) 2016. These guidelines ensure that the materials meet the required thermal standards, promoting energy efficiency and sustainable building practices.

For modeling purposes, the scenarios’ compositions are established into four types, each featuring different wall construction: wall 1 (BR), which refers to hollow brick and presents the baseline scenario; wall 2 (CN) refers to concrete hollow block; wall 3 (AD) refers to adobe brick; and wall 4 (ST) refers to limestone.

The parameters of the surfaces and building materials are performed using the ENVI-met database manager tool to ensure accurate simulations and analysis regarding outdoor thermal comfort. These comprehensive data were then compiled and saved as a software library, enabling easy access and future reference for modeling and further research.

Furthermore, the street scenarios (canyons) were initially designed based on the H/W ratio, which allows for the classification of three distinct types of street geometries: deep canyon (H/W = 1.25), normal canyon (H/W = 1), and shallow canyon (H/W = 0.62). These ratios were carefully derived, considering the actual height of buildings with adjustments made to the street width. Moreover, special attention was given to the orientation to design a series of canyons. They are strategically oriented in two principal directions: north–south and east–west. This thoughtful arrangement ensures comprehensive coverage of solar radiation from the sun’s path, effectively addressing different building façades and their solar exposure throughout the day (Figure 8).

In order to quantitatively evaluate the impact of building materials on outdoor thermal comfort, this study is based on the physiological equivalent temperature (PET) index, widely used as a thermal comfort measure. It is derived from the Munich Physiological Heat Balance (MEMI) model. Therefore, there are several advantages to using the PET index for urban climate studies: (1) it is universally applicable and remains unaffected by factors such as clothing values and metabolic activity values; (2) it is based on the principles of thermo-physiology, providing an accurate representation of how humans experience

climate sensations; (3) it operates without the necessity for subjective evaluations, relying solely on objective measures; and (4) it demonstrates sensitivity to windy environmental conditions. As a thermal measure, the PET index uses a specific scale depending on a set of criteria related to the direct physical environment and the human body. Accordingly, in this study, outdoor thermal comfort assessment follows the adapted PET scale for arid climate (BWh), as established by Cohen et al. (2019) [41].

Table 2. Thermal properties of the building materials.

Construction Materials	Layers (Outside to Inside)	Composition	Thickness (m)	Thermal Conductivity (W/m-K)	Specific Heat Capacity (J/kg K)	Density (kg/m ³)	Albedo	Emissivity	Absorption
Wall 1 (Reference)	Layer 1	Mortar	0.02	1.40	1080	2200	0.30	0.84	0.50
	Layer 2	Hollow brick	0.15	0.48	936	900	0.34	0.9	0.66
	Layer 3	Air cavity	0.05	0.024	1000	1.22	-	-	-
	Layer 4	Hollow brick	0.10	0.48	936	900	0.34	0.9	0.66
	Layer 5	Plaster	0.02	0.35	936	800	0.93	0.91	0.07
Wall 2	Layer 1	Mortar	0.02	1.40	1080	2200	0.30	0.94	0.50
	Layer 2	Concrete hollow block	0.20	1.10	1080	1300	0.30	0.92	0.80
	Layer 3	Plaster	0.02	0.35	936	800	0.93	0.91	0.07
Wall 3	Layer 1	Mortar	0.02	1.40	1080	2200	0.30	0.94	0.50
	Layer 2	Mud brick (adobe)	0.50	0.81	1075	2500	0.33	0.85	0.69
	Layer 3	Plaster	0.02	0.35	936	800	0.93	0.91	0.07
Wall 4	Layer 1	Mortar	0.02	1.40	1080	2200	0.3	0.94	0.50
	Layer 2	Lime stone	0.60	2.40	936	2400	0.4	0.95	0.50
	Layer 3	Plaster	0.02	0.35	936	800	0.93	0.91	0.07
Roof	Layer 1	Concrete	0.05	0.46	1080	1200	0.30	0.94	0.50
	Layer 2	Concrete slab (hollow block)	0.16	1.45	1080	1450	0.30	0.92	0.80
	Layer 3	Mortar	0.02	1.40	1080	2200	0.30	0.94	0.50
Street floor		Concrete pavement	0.01	-	-	-	0.50	0.90	-
		Asphalte Loamy soil	0.10	-	-	-	0.20	0.90	-

Further, the holistic modeling process using ENVI-met software involves field measurements conducted within the street canyon over eight months (from 10 April to 25 November 2021). In addition, the software implements the field measurement datasets using the full forcing method and converts all these input weather data into CSV files. Therefore, the chosen summer typical days were the 10–12 July 2021, representing the extreme weather period during the year within North African arid lands.

In many previous studies, numerical model results have been validated by comparing the results of simulations to in situ measurement data. According to Liu et al. (2021) [42], 92.59% of the previous studies used air temperature (T_a) as the primary variable for validation, followed by relative humidity (R_H) and mean radiant temperature (T_{mrt}) with 27.78% and 12.96%, respectively. On the other hand, surface temperature (T_s), air velocity (V_{air}), solar radiation (SR), and longwave radiation (LR) were chosen as less than 10% for the validation. In this regard, the validation step was performed with (T_a) using the root-mean-square error (RMSE), mean bias error (MBE), and linear regression (R^2) as statistical metrics methods. Basically, (RMSE), (MBE), and (R^2) are widely used statistical estimators that quantify the differences between observed and predicted data within mathematical approaches.

The evaluation of outdoor thermal comfort primarily relies on two meteorological variables: T_{mrt} , which is significantly impacted by various factors, including spatial configuration, shading effects, and the exposure of the human body to shortwave and longwave radiation fluxes [43]. Moreover, this study also considers surface temperature (T_s) concerning the direct and indirect effects of the surrounding building materials.

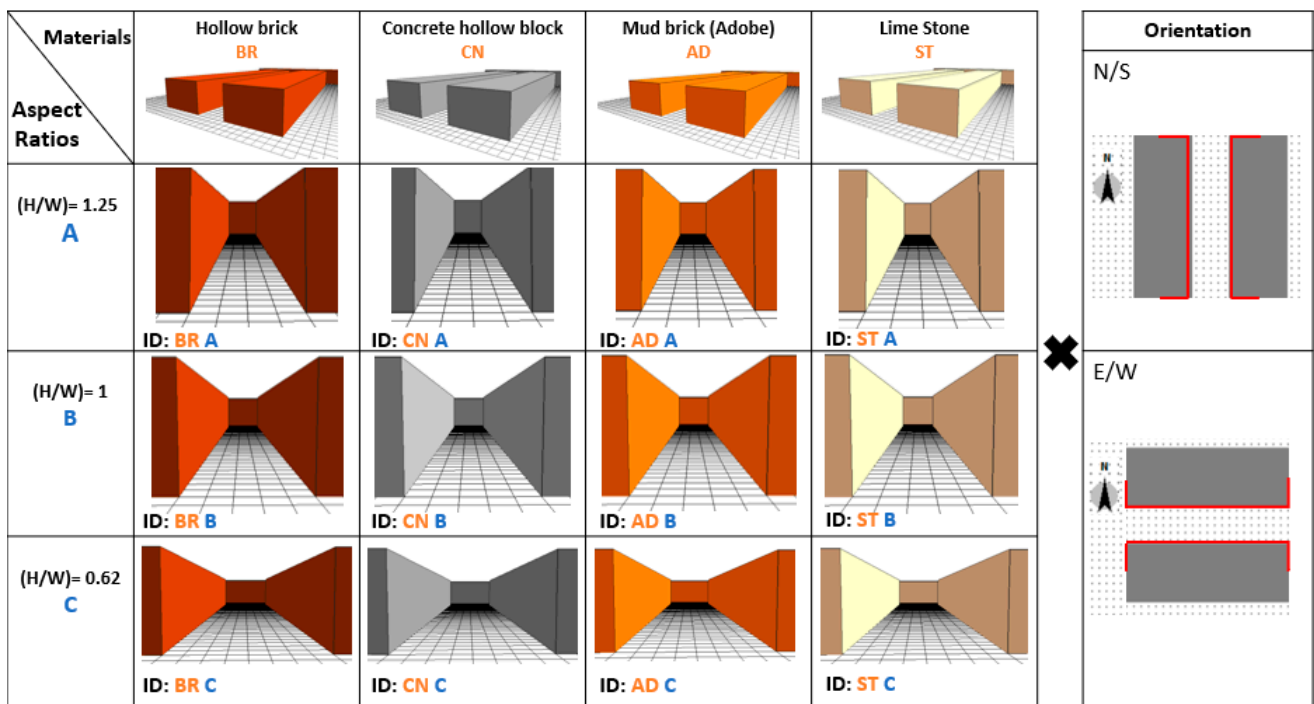


Figure 8. Development of 24 urban scenarios.

On the other hand, the PET index was determined utilizing BIO-met, which refers to a specific post-processing tool designed for human thermal comfort computation indices using simulated datasets generated with the ENVI-met model. BIO-met adheres to the specifications outlined in ISO 7730 [44], which define the ‘Standard Human’, ensuring its dependability and precision when evaluating individuals’ thermal comfort levels [45]. BIO-met can calculate various thermal indices based on the simulation data. It provides an assessment of dynamic thermal comfort (dPET) and a range of classic static indices such as the physiological equivalent temperature (PET), the standard effective temperature (SET), and the universal thermal climate index (UTCI). It should be noted that the adopted settings for the subject with BIO-met were a 35-year-old male person with a weight of 75 kg, a height of 1.75 m, a static clothing insulation outdoor (clo) of 0.90, and a total metabolic rate of about 86.21 W/m^2 in a standing position.

The simulation inputs process was based on various spatial characteristics, including location coordinates, model geometry, and construction material (Table 4). The simulation runtime was carried out to 48 h starting from 10 July 2021 to consider more valuable stability throughout the simulation process. The simulated output variables were also set at the pedestrian height (1.4 m).

2.5. Calibration with ENVI-Met

The RMSE and MBE were used for different comparisons between measured and simulated data with ENVI-met software. Table 3 outlines the RMSE and MBE calibration results, along with the validation of the numerical model, as shown in Equations (1) and (2).

Table 3. Statistical metrics for the validation of the numerical models.

Street	Indices	Reference Station	
Baseline	RMSE	1.34	5.08%
	MBE	0.76	2.88%

Table 4. ENVI-met modeling inputs parameters.

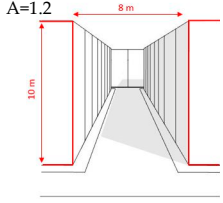
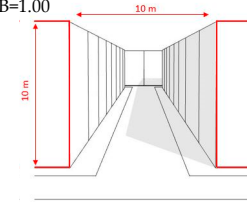
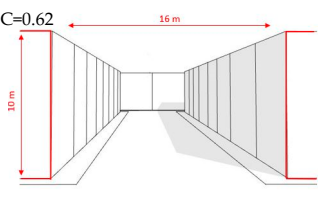
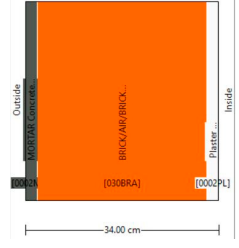
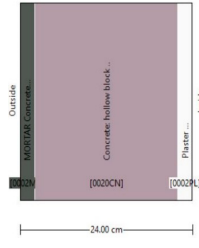
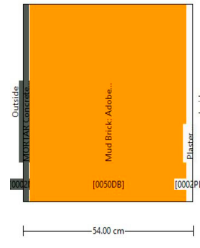
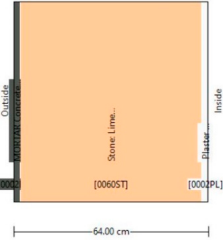
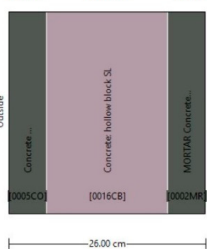
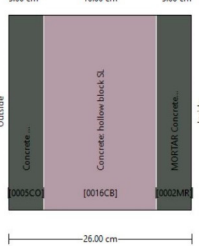
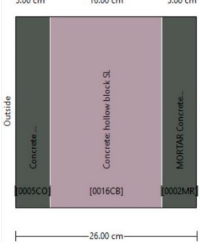
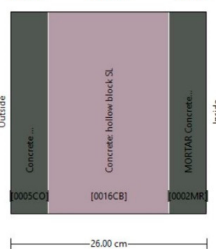
Space Geometry					
Street orientation	E-W N-S	E-W N-S	E-W N-S	E-W N-S	
Longitude (°)	5.73	5.73	5.73	5.73	
Latitude (°)	34.85	34.85	34.85	34.85	
Aspect Ratio (H/W)					
Model geometry					
Grid size	100 m × 70 m × 20 m	100 m × 70 m × 20 m	100 m × 70 m × 20 m	100 m × 70 m × 20 m	
dx = size of X grid	dx = 2.00	dx = 2.00	dx = 2.00	dx = 2.00	
dy = size of Y grid	dy = 2.00	dy = 2.00	dy = 2.00	dy = 2.00	
dz = size of Z grid	dz = 2.00	dz = 2.00	dz = 2.00	dz = 2.00	
Construction material					
Building material	<p>Walls: Created wall: Mortar; (hollow brick/ air/hollow brick); plaster</p> 	<p>Walls: Created wall: Mortar; concrete hollow block; plaster</p> 	<p>Walls: Created wall: Mortar; mud brick (adobe); plaster</p> 	<p>Walls: Created wall: Mortar; lime stone; plaster</p> 	
	<p>Roofs: Created roof: Concrete; concrete slab (hollow block); mortar</p> 	<p>Roofs: Created roof: Concrete; concrete slab (hollow block); mortar</p> 	<p>Roofs: Created roof: Concrete; concrete slab (hollow block); mortar</p> 	<p>Roofs: Created roof: Concrete; concrete slab (hollow block); mortar</p> 	
	Soil	Concrete pavement Asphalt Road Loamy soil	Concrete pavement Asphalt Road Loamy soil	Concrete pavement Asphalt Road Loamy soil	Concrete pavement Asphalt Road Loamy soil
	Simulation				
	Start date	10 July 2021	10 July 2021	10 July 2021	10 July 2021
	Start time	23 h 00	23 h 00	23 h 00	23 h 00
	Total simulation time	48 h	48 h	48 h	48 h
	Type of meteorological boundary conditions	Full forcing—CSV	Full forcing—CSV	Full forcing—CSV	Full forcing—CSV

Figure 9 shows a comparison between the measured and simulated air temperatures (T_a) for the conducted days. In the monitored period, the RMSE was 5.08%, and the MBE was 2.88%, while the admitted limit was $\pm 30\%$ and $\pm 10\%$, respectively. The model RMSE and MBE values for the hourly data were within ASHRAE-recommended hourly values as mentioned in the ASHRAE Standard 14-2002 [46].

$$\text{RMSE} = \sqrt{\frac{1}{n} \cdot \sum_{i=1}^n (\text{Sim}_i - \text{Obs}_i)^2} \quad (1)$$

$$\text{MBE} = \frac{1}{n} \cdot \sum_{i=1}^n (\text{Sim}_i - \text{Obs}_i) \quad (2)$$

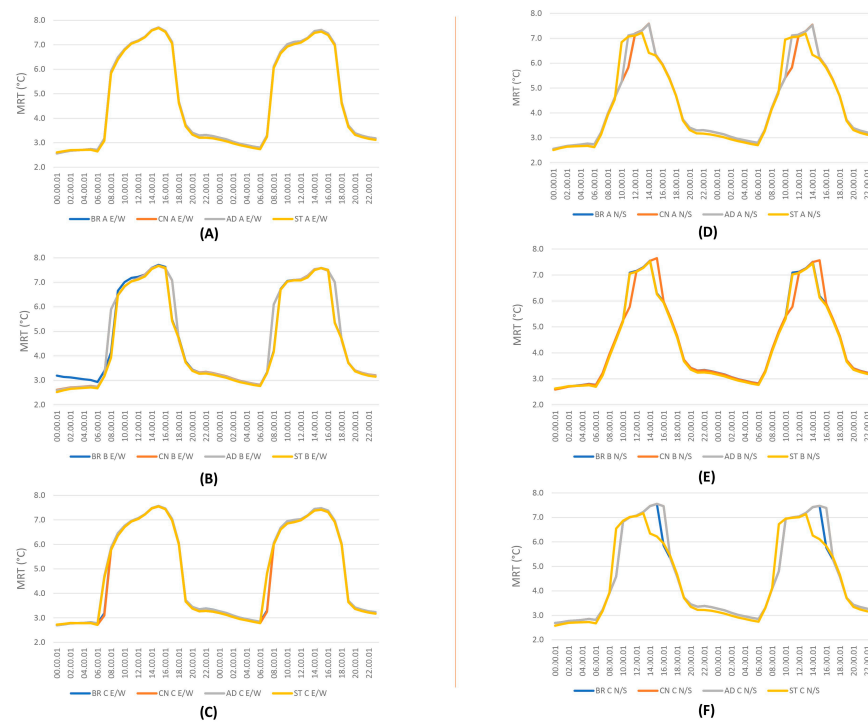


Figure 9. Hourly mean radiant temperature (MRT) values for the 24 scenarios: E-W (left) for the (A–C) ratio and N-S (right) for the (D–F) ratio.

3. Results

As explained, the 24 designed scenarios were simulated during the 10 and 11 July 2021, which refer to typical summer days within the studied context. The analysis of the microclimatic parameters was based on three main variables: T_{mrt} , T_s , and the PET index. It should be noted that all the values are representative of the measurement reference point.

3.1. Mean Radiant Temperature (T_{mrt})

Figure 9 displays a profile of the hourly average, maximum, and minimum T_{mrt} values obtained from the measuring point in the representational scenarios. Overall, the T_{mrt} values were roughly similar within the different street orientations, ratio aspects, and building materials effects, with a daily average of 48.1 °C in E-W and 44.2 °C in N-S orientations. The elevation of the variable was well observed during 12 continuous hours from 6:00 and started to decline gradually after 18:00, which is relatively related to solar radiation and insolation impacts. Therefore, in the E-W orientation, T_{mrt} maximums reached 77.1 °C in both scenarios' groups A ($H/W = 1$) and B ($H/W = 1.25$), and 75.7 °C in group C ($H/W = 0.62$) at 15:00. On the other hand, the north–south orientation values varied between: 75.9 °C in group A at 14:00 and 76.5 °C and 75.5 °C at 15:00 in groups B and C, respectively.

Exceptionally, the limestone (ST) within the N-S orientation, in both the A and C configuration groups, showed cooler T_{mrt} average values at peak hours (14:00). However, this same material displayed a more rapid increase in T_{mrt} values than the other materials at daytime hours, typically starting from 9:00 to 10:00, across all street geometries.

Although, in the E-W street orientation within the B aspect ratio, both brick (BR) and limestone (ST) scenarios were found to be the coolest materials with T_{mrt} values: 41.4 °C and 39.3 °C at 8:00 and 54.7 °C and 54.3 °C at 17:00, respectively. It should be noted that the differences between these two materials compared with concrete (CN) and adobe (AD) walls were approximately equal to $\Delta T_{mrt} = 19.2$ °C at 8:00 and $\Delta T_{mrt} = 16.6$ °C at 17:00.

As a result, the minimum T_{mrt} records were observed at nighttime hours with nearly similar values of 25.2 °C in the E-W orientation and 25.1 °C in the N-S orientation across all scenarios. Therefore, T_{mrt} gradually decreases after 19:00 to a minimum at 5:00 the following day.

Various reasons cause the elevation and differences in T_{mrt} during specific hours among all scenarios. The deep canyons (A and B) within the N-S orientation tend to be the coolest areas, where the brick and limestone walls are less hot. This was possible because the aspect ratios provide more shading and light materials that absorb less solar radiation.

Additionally, the E-W street orientation fronts solar radiation during the daytime cycle, causing higher T_{mrt} , contrary to the N-S orientation, which is less exposed to solar radiation and provides more shaded surfaces.

3.2. Surface Temperature (T_s)

The simulation results for the T_s of walls in both street façades at the height of 1.4 m within all modeled scenarios are reported as box plots (Figures 10 and 11). As a result, there is a substantial similarity in the walls' thermal behavior during different measured periods. The median T_s obtained during 24 h is between 37.3 °C in the E-W street orientation and 39.9 °C in the N-S street orientation, respectively. It should be noted that the sides of the façades are opposite to the street orientations, i.e., in the E-W street orientation, the buildings' façades face the north and south sides, and vice versa (Appendix A).

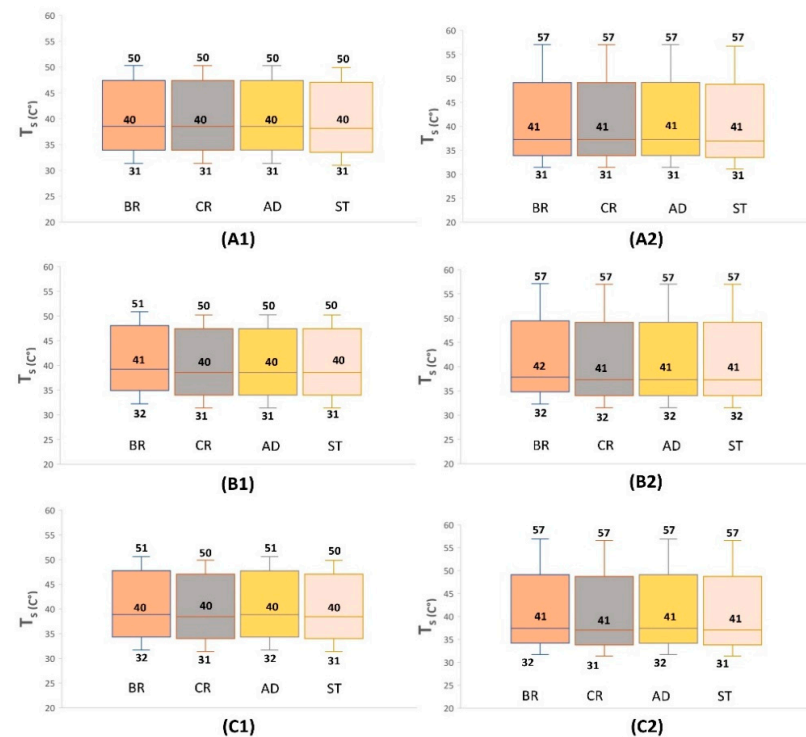


Figure 10. Box plots of surface temperature (T_s) values: E-W orientation for the (A–C) ratios, (A1,B1,C1) for the north side, and (A2,B2,C2) for the south side.

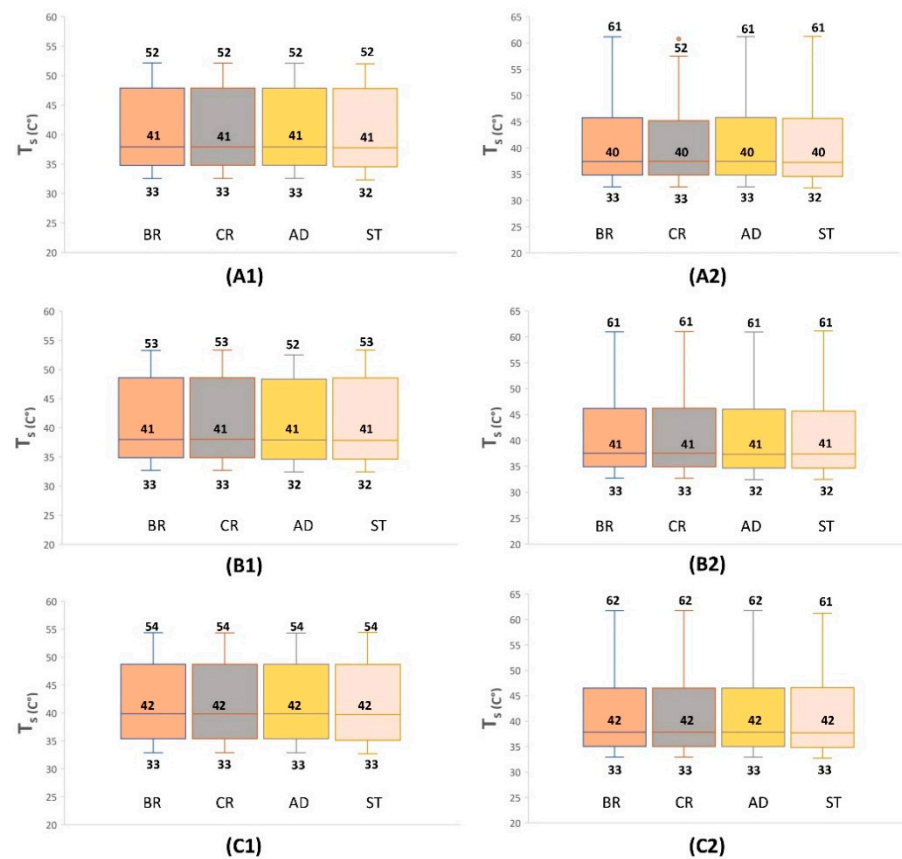


Figure 11. Box plots of surface temperatures (T_s) values: N-S orientation for the (A–C) ratios (A1,B1,C1) for the east side and (A2,B2,C2) for the west side.

Among all E-W street orientation scenarios, on the north side façade, 50% of the T_s averages over 12 h fell within the range of 34 °C to 47 °C, whereas the median value remained below 25%. On the south side façade, the ranges were slightly higher, and 50% of the T_s results varied between 34 °C and 49 °C, whereas the median was below the mean value of 41 °C. Accordingly, the T_s averages across all wall models were quite similar on both façades sides, with a very slight difference observed in the limestone (ST) scenario, which was slightly cooler compared with the other materials.

On the other hand, the N-S street orientation scenarios revealed higher T_s averages compared with the E-W orientation, with maximum values reaching 62 °C. On the east side, 50% of the values were between 35 °C and 49 °C, whereas the median was below 42 °C. Therefore, on the west side, 50% of the obtained T_s averages fell into the range of 35 °C to 47 °C, and 25% occurred from 47 °C to 62 °C.

Similar to the E-W orientation, the limestone (ST) remains the cooler material with a slight difference of 1 °C compared with the other building materials.

In this regard, deep ($H/W = 1.25$ and 1) and shallow ($H/W = 0.62$) canyons displayed similar T_s averages during the 24-hour daily cycle. Surprisingly, there was no significant cooling effect from the light materials (BR, AD, and ST) that can absorb less solar radiation, and the surface temperature of the walls was greatly influenced by short-wave radiation. In this case, orientation can play a critical factor in either increasing or slightly decreasing the thermal behavior of the materials, depending on the material absorption and the albedo properties.

Moreover, without an important and essential shading profile on the street, the thermal behavior of walls may remain unchanged. The thermal properties of the building materials within deep or shallow canyons cannot influence it. Furthermore, continuous exposure to solar radiation during the day reduces the thermal cool-down of the building material and elevates the urban heat island inside effects within the streets.

3.3. The Physiological Equivalent Temperature Index (PET)

The assessment of the PET index showed high values during the studied period featuring three different thermal stress zones (Figure 12): warm, hot, and very hot. The PET ranges were based on the study by (Cohen et al., 2019) [41] in arid climates (BWh). In this regard, the present PET results are related to 11 July 2021. Thus, the results showed increased PET values during the daytime hours from sunrise until sunset within all scenarios.

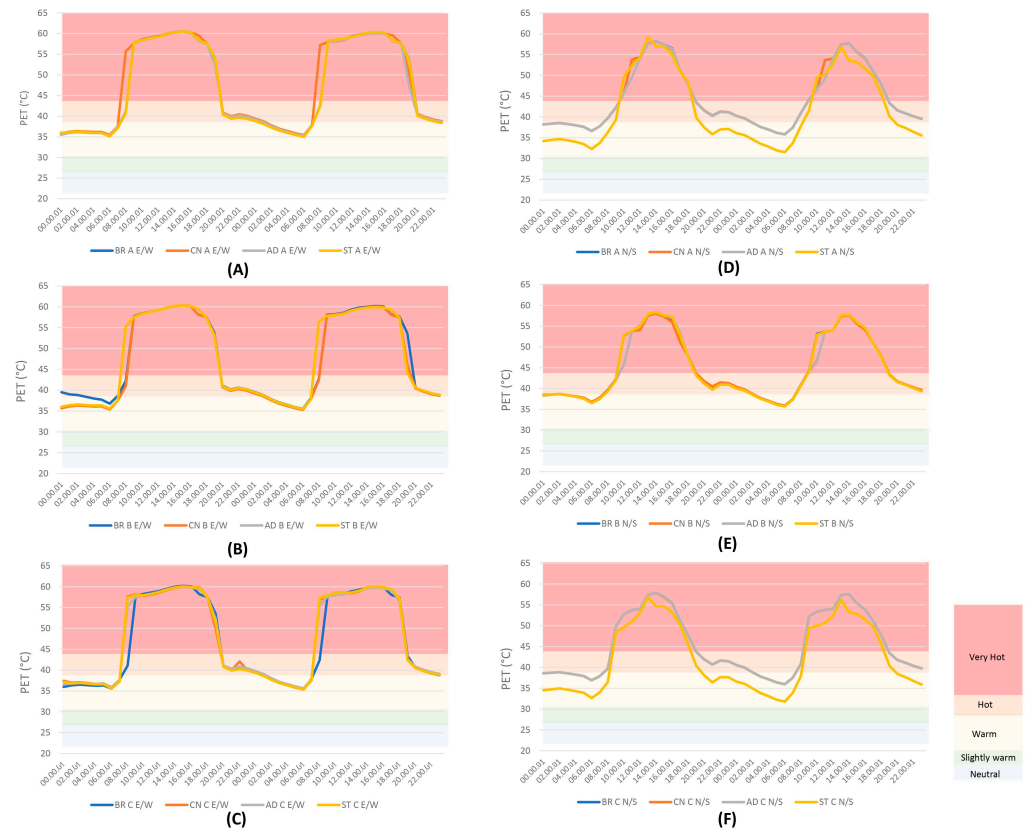


Figure 12. Hourly PET values for the 24 scenarios: E-W (left) for the (A–C) ratio and N-S (right) for the (D–F) ratio.

Therefore, among the E-W street orientation through the deep canyons (A ‘H/W = 1.25’, and B ‘H/W = 1’) and the shallow canyon C (H/W = 0.62), all the modeled materials experienced warm thermal stress during the period between 00:00 and 6:00, except the reference brick wall (BR) within H/W = 1, which experienced hot thermal stress during the same time. Accordingly, these street cases revealed a near similarity within all materials on the PET values with a difference equal to $\Delta PET_{E-W} = 0.3$ °C. The highest PET value was obtained at 15:00 with a $PET_{maxE-W} = 60.6$ °C when the period between 9:00 and 19:00 was extremely heat stress. The average values of PET were 47.7 °C with extreme hot stress. Afterward, PET values gradually decreased and reached 37 °C after midnight of the next day. Otherwise, the thermal stress hours’ rates varied between warm, hot, and extreme heat stress with 20.3%, 30.6%, and 49.1% respectively, during the day. Some exceptions on the thermal stress experienced between street orientations, ratios, and materials’ thermal behavior include 8% of warm stress in scenario ‘E-W, B, BR’ and 27.1% of hot stress in scenario ‘E-W, A, CN’. Further, similar results occurred on 12 July 2021 (Figure 13). It should be indicated that no significant cooling effect or optimal situation was observed from the building materials along all streets’ ratios in the E-W orientation. This lack of a cooling effect can be attributed to the high solar exposure quantity and highlights the necessity of shading canopies. Even during nighttime hours, the minimum average value recorded was $PET_{minE-W} = 35.1$, indicating warm thermal stress. In such cases, an unshaded deep or

shallow canyon oriented to the E-W direction may not benefit from the cooling effect of building properties. It could contribute to a warming effect during a summer day.

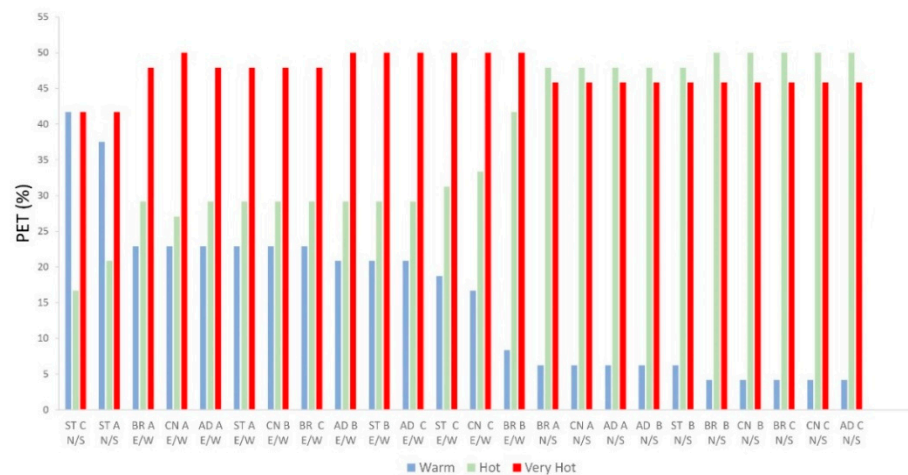


Figure 13. Variation in human thermal stress levels within the 24 scenarios.

On the other hand, the N-S street orientation displayed high PET values within the A, B, and C canyons geometries. It also revealed hot thermal stress between 00:00 and 08:00, except for the limestone wall (ST) scenario, which experienced warm stress during the same time along the deep and shallow canyons. The results varied from a maximum $PET_{\max N-S} = 59.2$ °C at 13:00 and a minimum $PET_{\min N-S} = 32.2$ °C at 6:00, whereas the daily average value through all scenarios was $PET_{\text{average}N-S} = 44.6$ °C. Furthermore, the PET values within the different ratios and wall materials were near each other during the daily cycle.

Regarding human-perceived sensation, the thermal stress variation ranged from the warm to cooler range, hot, and extreme heat stress with daily average rates of 10.9%, 43.9%, and 45.1%, respectively.

Remarkably, the limestone wall (ST) scenario showed the highest rates of the warm thermal range, with 37.5% in the A canyon group and 41.7% in the C canyon group. Conversely, the same wall scenario featured the lowest rates of the hot thermal range, with 20.8% in the A canyon group and 16.7% in the C canyon group similarly, the lowest rate of extreme heat stress with 41.7% within both A and C canyons. Surprisingly, with a H/W = 1, the B deep canyon did not contribute to patterns similar to those of the other canyon forms.

In this context, the N-S street orientation had cooler thermal sensations than the E-W orientation. The thermal performance of the building materials was more efficient in responding to the N-S than the E-W orientation. This latter result can be related to the influence of solar exposure and shade advantages provided by the street orientation. These factors can protect the building façade and the street sidewalks from direct radiation.

Furthermore, limestone remains an effective material for mitigating heat stress inside urban canyons. While the observed effect was minimal, it did result in an approximate improvement in human thermal comfort within the canyons, even in the absence of shading devices.

As observed in the current study, the variation in the thermal behavior of walls strongly influenced the outdoor thermal comfort within a typical urban canyon. The results indicated two distinct categories of materials: cold materials with a slow response to heat diffusing from the nearby environment and hot materials that rapidly absorb and retain heat (Figure 14). This distinction depended highly on the street orientation and the canyon ratio aspect, classifying materials into different cool and hot categories.

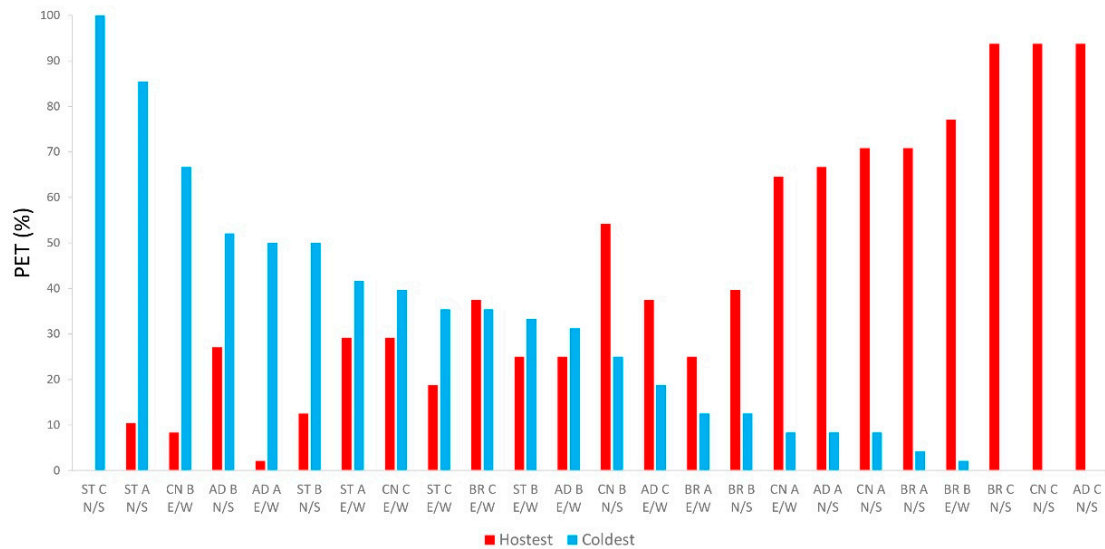


Figure 14. Thermal behavior of the externally modeled walls.

Accordingly, this gradation of scenarios thermal behavior characterized six different categories as follows:

- High cooling category: [above 60–100%] of cooling efficiency, obtained predominantly in the N-S orientation in the A ($H/W = 1.25$) and C ($H/W = 0.62$) canyon groups and the E-W orientation in the B ($H/W = 1$) canyon group. Limestone (ST) was a prominent material in this category.
- Medium cooling category: [40–60%] of cooling efficiency, observed in both orientations in the deep canyons A and B for limestone (ST) and adobe (AD) walls.
- Low cooling category: [below 40%] of cooling efficiency, notably observed in the E-W orientation in the shallow canyon, with brick (BR) and concrete (CN) being the most affected materials.
- Extreme heating category: [above 60–100%] of heat retention predominantly occurred in the N-S orientation within all canyon forms. The most affected materials were brick (BR), concrete (CN), and slightly, adobe (AD).
- Medium heating category: [40–60%] of heat retention, obtained solely with the concrete (CN) wall in the N-S orientation in B canyon.
- Low heating category: [below 40%] of heat retention, varied between the E-W and N-S orientations across different canyon forms and walls.

4. Discussion

This section offers a concise overview of the key research findings, emphasizing recommendations, strengths, limitations, and implications for both practical application and future research.

The current study provides an original methodology for calculating the correlation between street geometries and the thermal performance of building materials under extreme weather conditions to assess outdoor thermal comfort, utilizing multiple designed scenarios.

4.1. Findings and Recommendations

The study findings indicate that outdoor thermal comfort is strongly affected by the urban geometry of a canyon undergoing specific thermal properties of external materials of the surrounding buildings.

As a key result, the materials' thermal characteristics play a primary factor in controlling the spatial and temporal thermal behavior inside urban canyons. They may generate cooling and overheating during important periods of the day. For instance, limestone can provide a cooling efficiency range of 85% to 100% in deep and shallow canyons in the N-S

orientation. In contrast, brick walls can cause a heat retention range varying from 70% to 93% in the same canyons (Table 5).

Table 5. Building materials' external thermal efficiency related to the H/W ratio and street orientation.

Categories		Canyon A (H/W = 1.25)				Canyon B (H/W = 1)				Canyon C (H/W = 0.62)			
		BR	CN	AD	ST	BR	CN	AD	ST	BR	CN	AD	ST
Cooling efficiency	E-W	∇12.5%	∇8.3%	∇50.0%	∇41.7%	∇2.1%	∇66.7%	∇31.3%	∇33.3%	∇35.4%	∇39.6%	∇18.8%	∇35.4%
Heat retention		Δ25.5%	Δ64.6%	Δ2.1%	Δ29.2%	Δ77.1%	Δ8.3%	Δ25.0%	Δ25.0%	Δ37.5%	Δ29.2%	Δ37.5%	Δ18.8%
Cooling efficiency	N-S	∇4.2%	∇8.3%	∇8.3%	∇85.4%	∇12.5%	∇25.0%	∇50.0%	∇50.0%	∇0.0%	∇0.0%	∇0.0%	∇100.0%
Heat retention		Δ70.8%	Δ70.8%	Δ66.7%	Δ10.4%	Δ39.6%	Δ54.2%	Δ27.1%	Δ12.5%	Δ93.8%	Δ93.8%	Δ93.8%	Δ0.0%
Thermal perception													
Warm	E-W	22.9%	22.9%	22.9%	22.9%	8.3%	22.9%	20.8%	20.8%	22.9%	16.7%	20.8%	18.8%
	N-S	6.3%	6.3%	6.3%	37.5%	4.2%	4.2%	6.3%	6.3%	4.2%	4.2%	4.2%	41.7%
Hot	E-W	29.2%	27.1%	29.2%	29.2%	41.7%	29.2%	29.2%	29.2%	29.2%	33.3%	50.0%	31.3%
	N-S	47.9%	47.9%	47.9%	20.8%	50.0%	50.0%	47.9%	47.9%	50.0%	50.0%	50.0%	16.7%
Extreme heat	E-W	47.9%	50%	47.9%	47.9%	50%	47.9%	50%	50%	47.9%	50%	50%	50%
	N-S	45.8%	45.8%	45.8%	41.7%	45.8%	45.8%	45.8%	45.8%	45.8%	45.8%	45.8%	41.7%
PET (°C)				17–26		26–28		28–37		37–42		>42	
				Neutral		Slightly warm		Warm		Hot		Very hot	
Thermal comfort stress level				No thermal stress		Slight heat stress		Moderate heat stress		Strong heat stress		Extreme heat stress	

Albedo and absorption are crucial parameters influencing surface temperatures and outdoor thermal comfort within urban canyons. A high albedo value with a low absorption value can help to reduce 50% of outdoor human thermal discomfort in extreme weather conditions, and vice versa.

In similar cases, the differences between maximum and minimum thermal stress levels can reach 16 °C during the same hours, notably, during sunrise and sunset phases.

The effectiveness of building materials in influencing outdoor thermal comfort cannot be solely attributed to specific light or cool materials. Instead, it depends on a canyon's geometry and orientation. Notably, the orientation that is most susceptible to overheating is the N-S when building façades face east and west. This latter result is primarily due to the daily cycle of solar radiation.

In relation to the H/W ratio and canyon orientation, there are six distinct categories of building materials, each with its impact on outdoor thermal comfort: (i) high cooling, (ii) medium cooling, (iii) low cooling, (iv) high heating, (v) medium heating, and (vi) low heating material.

Without shading canopies, the thermal efficiency of building material is strongly limited and undergoes solar radiation intensity within deep and shallow canyons. Accordingly, a shallow canyon can benefit from rapid cooling of the stored heat retention versus a deep canyon during nighttime hours. However, they face large exposure to direct solar radiation during daytime hours. For example, using limestone with H/W = 1.25 in the N-S orientation can result in hot stress levels of 20.8% compared with 16.7% with H/W = 0.62.

Increasing the H/W aspect ratio can significantly improve thermal comfort in the summer due to shading. However, the effectiveness of this strategy may vary depending on canyon orientation and the type of external building envelope.

Over all the designed scenarios, the most effective bioclimatic passive strategy that could result is the E-W orientation, with H/W < 1, characterized by high albedo building material, similar to the E-W C scenario, within limestone.

4.2. Strength and Limitations

This study's strength relates to the novel categorization of the outdoor thermal impact of building materials concerning urban canyon geometries. It was very limited before a study brought together the correlation between street orientation, aspect ratio, and building thermal properties, which was rarely gathered as three key factors that affect human thermal comfort in outdoor areas, specifically in arid environments. This multi-variable formula enables a comprehensive analysis of building architecture and urban planning.

Determining design rules of streets for pedestrian comfort relies on the three-variable formula comprising street orientation, aspect ratio, and thermal properties of building materials to achieve optimal or nearly optimal human thermal comfort, particularly in extreme weather conditions. To the best of our knowledge, few studies have explored the coupling of two of the three variables to improve the outdoor thermal environment.

This study used a coupled methodology between field measurements and 24 numerical calibrated models using ENVI-met software. Consequently, this series of scenarios enables a comprehensive understanding of the spatial and temporal thermal behavior of pedestrians throughout various canyon forms in the city. The applied approach helps characterize optimal pedestrian walkability strategies and promote outdoor human interactions.

However, it is essential to note that this study has several limitations. For instance, this study could not obtain solar radiation requirements due to the unavailability of suitable measurement instruments. Solar radiation levels could be incorporated into the model's calibration steps to enhance the accuracy of the obtained data. Moreover, a more exhaustive approach could involve measuring RGB color texture temperatures for uncertainty analysis, providing a more accurate understanding of the impact of the thermal properties of building materials. Determining whether the color texture is cool or warm could identify the most effective materials in terms of color for optimal thermal properties. This study did not include wall finishes, which could strongly affect outdoor thermal comfort by influencing the elevation of the external surface temperature and radiant heat during daytime hours. Furthermore, conducting an annual analysis throughout the year would allow us to determine optimal design solutions for the three studied variables. Long-term analysis enhances the understanding of the thermal behavior of building materials under various weather conditions.

4.3. Implication for Practice and Research

This study's outcomes help to identify the most effective street configuration for extreme weather conditions. We believe architects, urban planners, and decision-makers can apply these findings to enhance outdoor thermal comfort in the early design and planning stages. This can be achieved by coupling street geometry with building envelope solutions.

The presented tables and figures enable architects and urban planners to apply adequate geometric and parametric aspects for street configurations and assess the need for specific methods using an adaptive model suitable for arid climates. Another significant implication of this study is the necessity for revised categorization of building materials, mainly focusing on their thermal properties. The National Building Efficiency Standard of Algeria (CNERIB) must be updated to reflect these findings. Therefore, we believe it is crucial to engage with code officials, specifically on the Building Energy Regulations document (DTR), to encourage the adoption and implementation of our recommendations, which will have a significant impact on the professional practice of urban design adaptation. Future research should prioritize continuously measuring the thermal behavior of building materials in each climatic zone of Algeria and developing climate-specific design parameters. A new categorization of effective building materials should be adapted to diverse climate zones and their characteristics for the long term.

5. Conclusions

The outdoor thermal comfort in diverse street canyon configurations during summer typical days was investigated in the case of Biskra City, Algeria. Current urban design in

Algeria does not account for pedestrian outdoor thermal comfort. Therefore, various urban design and landscape architecture practices are necessary to address the urban heat island effect and the impact of climate change.

Continuous data from the measurement station within an urban canyon in Biskra City were used as inputs to the ENVI-met software modeling. The PET index was computed as an outdoor thermal comfort parameter. Additionally, 24 H/W aspect ratio canyon orientation scenarios with building material characteristics were simulated.

Achieving an optimal outdoor thermal comfort threshold is challenging due to various factors, including building materials and street geometry properties, such as albedo, the H/W ratio, and street orientation. These factors all play significant roles in increasing or decreasing outdoor thermal comfort.

Comparing the different scenarios shows that thermal stress mitigation is not solely dependent on whether a canyon is deep or shallow. It significantly hinges on the street orientation and the nature of the building materials. Therefore, in similar arid climates, the coupling of the H/W ratio and street orientation reveals six distinct categories of building materials, each of which has a unique impact on outdoor thermal comfort and can be applied in urban design practices: (i) high cooling, (ii) medium cooling, (iii) low cooling, (iv) high heating, (v) medium heating, and (vi) low heating material.

Utilizing cool materials such as limestone or adobe to reduce thermal stress within urban canyons may not be an effective passive strategy without considering the H/W ratio and orientation aspects. Shading can be an effective element in arid climates to ensure neutral thermal ranges for pedestrians. This is why the H/W aspect ratio and street orientation strongly influence the thermal behavior of building envelopes.

The findings also demonstrate that, due to the extreme weather conditions being far from what is deemed a comfortable range in summer, it is impossible to consistently achieve optimal outdoor thermal comfort using only passive techniques at all times, even with a combination of short-term and long-term strategies. However, the urban strategies suggested in this study would help mitigate the severity of the thermal discomfort that people might experience due to extreme heat. Given Algerian considerations, providing a neutral range of outdoor thermal comfort is important.

This research has contributed to urban design and policy and provided guidelines for strategies under extreme summer weather conditions. Future research could investigate the external effects of different building material characteristics in diverse climate zones with varying urban design regulations. Furthermore, investigating the effects of various scenarios coverages and building envelopes could help define more precise and effective strategies. The inclusion of various shading canopies and tree plantings should also be considered in future studies.

Author Contributions: Conceptualization, F.Z.B.R., A.A., S.B. and M.E.M.; methodology, F.Z.B.R., A.A., G.S., S.B., W.A.M. and M.E.M.; software, F.Z.B.R. and M.E.M.; validation, F.Z.B.R., A.A. and M.E.M.; formal analysis, F.Z.B.R., A.A., G.S. and M.E.M.; investigation, F.Z.B.R. and M.A.E.B.R.; resources, F.Z.B.R.; data curation, F.Z.B.R.; writing—original draft preparation, F.Z.B.R.; writing—review and editing, F.Z.B.R., W.A.M. and M.E.M.; visualization, F.Z.B.R., M.A.E.B.R. and M.E.M.; supervision, A.A., G.S., S.B. and M.E.M.; project administration, F.Z.B.R., A.A. and M.E.M.; funding acquisition, F.Z.B.R., W.A.M. and M.E.M. All authors have read and agreed to the published version of the manuscript.

Funding: This research received no external funding.

Institutional Review Board Statement: Not applicable.

Informed Consent Statement: Not applicable.

Data Availability Statement: Data are available upon request.

Acknowledgments: We would like to acknowledge the LACOMOFA Laboratory, University of Biskra, and the Department of Energy, Systems, Territory and Construction Engineering, University of Pisa, Italy, for the use of the monitoring equipment in this research and valuable support during the experiments and data analysis process. The authors would also like to thank the University of Pisa, Italy, for the scientific stay in the Department of Energy, Systems, Territory, and Construction Engineering, under the Erasmus + KA 107 Program 2022–2023 and their assistance in administrative procedures.

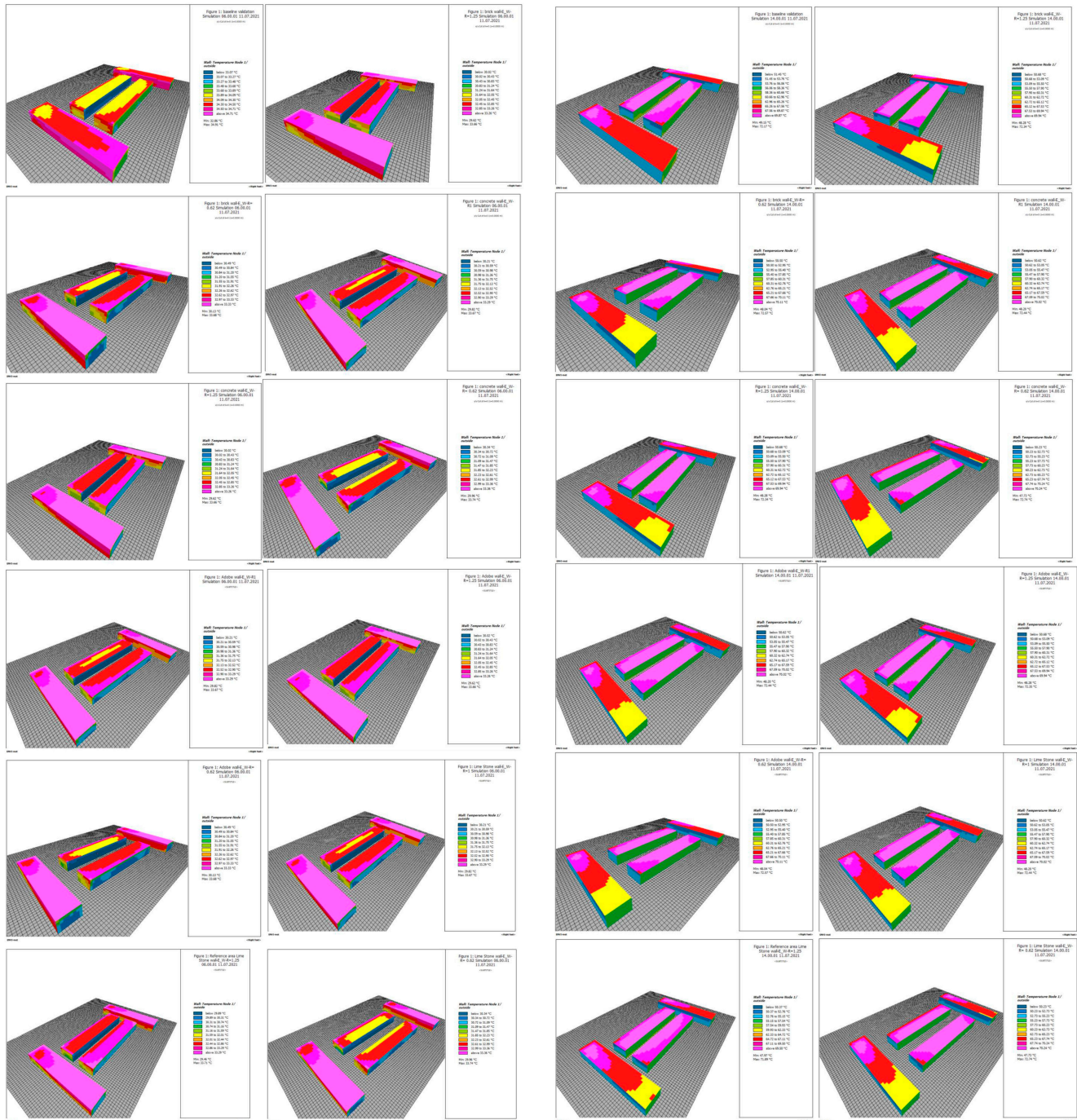
Conflicts of Interest: The authors declare no conflicts of interest.

Nomenclature

The following abbreviations are used in this paper:

ASHRAE	American Society of Heating, Refrigerating, and Air-Conditioning Engineers
CBE	Berkeley Center for the Built Environment
CNERIB	Algerian Centre for Building Integrated Studies and Research
BR	hollow brick wall
CN	concrete hollow block wall
AD	adobe brick wall
ST	limestone wall
PET	physiological equivalent temperature
T_{mrt}	mean radiant temperature
T_s	surface temperature
T_a	air temperature
CFD	computational fluid dynamics
MBE	mean bias error
RMSE	root mean square error

Appendix A



(a)

(b)

Figure A1. Surface temperature (T_s) values in the E-W orientation: (a) refers to the north façade and (b) refers to the south façade of buildings using the Leonardo interface.

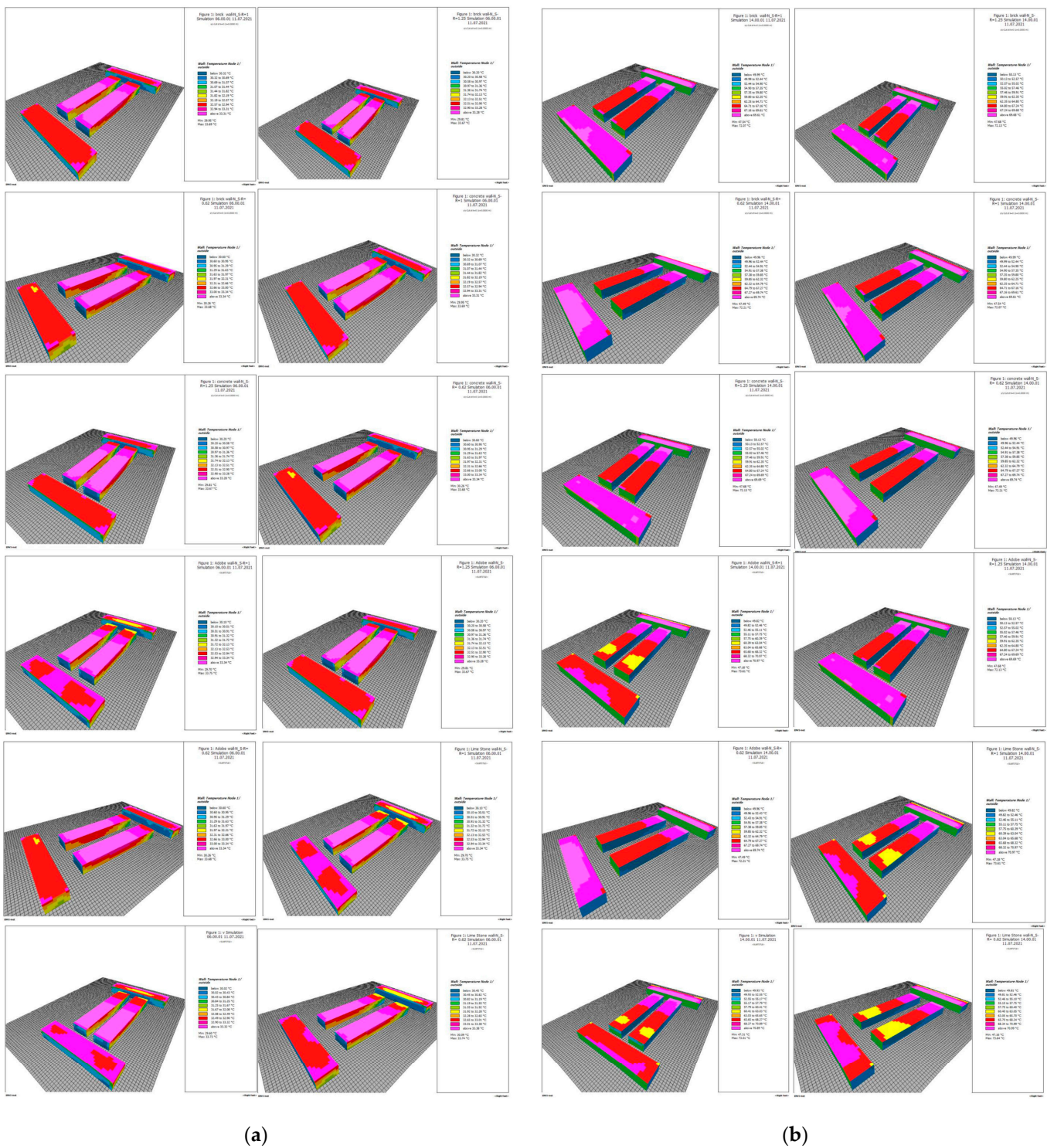


Figure A2. Surface temperature (T_s) values in the N-S orientation: (a) refers to the east façade and (b) refers to the west façade of buildings using the Leonardo interface.

References

1. Kleerekoper, L.; Van Esch, M.; Salcedo, T.B. How to make a city climate-proof, addressing the urban heat island effect. *Resour. Conserv. Recycl.* **2012**, *64*, 30–38. [[CrossRef](#)]
2. Rydin, Y.; Bleahu, A.; Davies, M.; Dávila, J.D.; Friel, S.; De Grandis, G.; Groce, N.; Hallal, P.C.; Hamilton, I.; Howden-Chapman, P.; et al. Shaping cities for health: Complexity and the planning of urban environments in the 21st century. *Lancet* **2012**, *379*, 2079–2108. [[CrossRef](#)] [[PubMed](#)]

3. Magli, S.; Lodi, C.; Lombroso, L.; Muscio, A.; Teggi, S. Analysis of the urban heat island effects on building energy consumption. *Int. J. Energy Environ. Eng.* **2015**, *6*, 91–99. [[CrossRef](#)]
4. Pérez-Lombard, L.; Ortiz, J.; Pout, C. A review on buildings energy consumption information. *Energy Build.* **2008**, *40*, 394–398. [[CrossRef](#)]
5. Darbani, E.S.; Rafieian, M.; Parapari, D.M.; Guldmann, J.M. Urban design strategies for summer and winter outdoor thermal comfort in arid regions: The case of historical, contemporary and modern urban areas in Mashhad, Iran. *Sustain. Cities Soc.* **2023**, *89*, 104339. [[CrossRef](#)]
6. Ali-Toudert, F. Exploration of the thermal behaviour and energy balance of urban canyons in relation to their geometrical and constructive properties. *Build. Environ.* **2021**, *188*, 107466. [[CrossRef](#)]
7. Castaldo, V.L.; Rosso, F.; Golasi, I.; Piselli, C.; Salata, F.; Pisello, A.L.; Ferrero, M.; Cotana, F.; de Lieto Vollaro, A. Thermal comfort in the historical urban canyon: The effect of innovative materials. *Energy Procedia* **2017**, *134*, 151–160. [[CrossRef](#)]
8. Andreou, E.; Axarli, K. Investigation of urban canyon microclimate in traditional and contemporary environment. Experimental investigation and parametric analysis. *Renew. Energy* **2012**, *43*, 354–363. [[CrossRef](#)]
9. Erell, E.; Pearlmutter, D.; Boneh, D.; Kutiel, P.B. Effect of high-albedo materials on pedestrian heat stress in urban street canyons. *Urban Clim.* **2014**, *10*, 367–386. [[CrossRef](#)]
10. Kolokotsa, D.; Santamouris, M.; Zerefos, S.C. Green and cool roofs' urban heat island mitigation potential in European climates for office buildings under free floating conditions. *Sol. Energy* **2013**, *95*, 118–130. [[CrossRef](#)]
11. Santamouris, M. Using cool pavements as a mitigation strategy to fight urban heat island—A review of the actual developments. *Renew. Sustain. Energy Rev.* **2013**, *26*, 224–240. [[CrossRef](#)]
12. Rosso, F.; Jin, W.; Pisello, A.L.; Ferrero, M.; Ghandehari, M. Translucent marbles for building envelope applications: Weathering effects on surface lightness and finishing when exposed to simulated acid rain. *Constr. Build. Mater.* **2016**, *108*, 146–153. [[CrossRef](#)]
13. Deng, J.Y.; Wong, N.H. Impact of urban canyon geometries on outdoor thermal comfort in central business districts. *Sustain. Cities Soc.* **2020**, *53*, 101966. [[CrossRef](#)]
14. Johansson, E. Influence of urban geometry on outdoor thermal comfort in a hot dry climate: A study in Fez, Morocco. *Build. Environ.* **2006**, *41*, 1326–1338. [[CrossRef](#)]
15. Ali-Toudert, F.; Mayer, H. Numerical study on the effects of aspect ratio and orientation of an urban street canyon on outdoor thermal comfort in hot and dry climate. *Build. Environ.* **2006**, *41*, 94–108. [[CrossRef](#)]
16. Muniz-Gaal, L.P.; Pezzuto, C.C.; de Carvalho, M.F.H.; Mota, L.T.M. Urban geometry and the microclimate of street canyons in tropical climate. *Build. Environ.* **2020**, *169*, 106547. [[CrossRef](#)]
17. Wonorahardjo, S.; Sutjahja, I.M.; Mardiyati, Y.; Andoni, H.; Thomas, D.; Achsani, R.A.; Steven, S. Characterising thermal behaviour of buildings and its effect on urban heat island in tropical areas. *Int. J. Energy Environ. Eng.* **2020**, *11*, 129–142. [[CrossRef](#)]
18. Rosso, F.; Golasi, I.; Castaldo, V.L.; Piselli, C.; Pisello, A.L.; Salata, F.; Ferrero, M.; Cotana, F.; de Lieto Vollaro, A. On the impact of innovative materials on outdoor thermal comfort of pedestrians in historical urban canyons. *Renew. Energy* **2018**, *118*, 825–839. [[CrossRef](#)]
19. Schrijvers, P.J.C.; Jonker, H.J.J.; De Roode, S.R.; Kenjereš, S. The effect of using a high-albedo material on the Universal Temperature Climate Index within a street canyon. *Urban Clim.* **2016**, *17*, 284–303. [[CrossRef](#)]
20. Matzarakis, A.; Mayer, H.; Iziomon, M.G. Applications of a universal thermal index: Physiological equivalent temperature. *Int. J. Biometeorol.* **1999**, *43*, 76–84. [[CrossRef](#)]
21. Höppe, P. The physiological equivalent temperature—a universal index for the biometeorological assessment of the thermal environment. *Int. J. Biometeorol.* **1999**, *43*, 71–75. [[CrossRef](#)] [[PubMed](#)]
22. Potchter, O.; Cohen, P.; Lin, T.P.; Matzarakis, A. Outdoor human thermal perception in various climates: A comprehensive review of approaches, methods and quantification. *Sci. Total Environ.* **2018**, *631*, 390–406. [[CrossRef](#)] [[PubMed](#)]
23. Staiger, H.; Laschewski, G.; Matzarakis, A. Selection of appropriate thermal indices for applications in human biometeorological studies. *Atmosphere* **2019**, *10*, 18. [[CrossRef](#)]
24. Bruse, M. ENVI-Met 3.0: Updated Model Overview. University of Bochum. 2004. Available online: www.envi-met.com (accessed on 15 November 2023).
25. Salata, F.; Golasi, I.; de Lieto Vollaro, R.; de Lieto Vollaro, A. Urban microclimate and outdoor thermal comfort. A proper procedure to fit ENVI-met simulation outputs to experimental data. *Sustain. Cities Soc.* **2016**, *26*, 318–343. [[CrossRef](#)]
26. Labdaoui, K.; Mazouz, S.; Acidi, A.; Cools, M.; Moeinaddini, M.; Teller, J. Utilizing thermal comfort and walking facilities to propose a comfort walkability index (CWI) at the neighbourhood level. *Build. Environ.* **2021**, *193*, 107627. [[CrossRef](#)]
27. Jia, S.; Wang, Y. Effect of heat mitigation strategies on thermal environment, thermal comfort, and walkability: A case study in Hong Kong. *Build. Environ.* **2021**, *201*, 107988. [[CrossRef](#)]
28. Mouada, N.; Zemmouri, N.; Meziani, R. Urban morphology, outdoor thermal comfort and walkability in hot, dry cities: Case study in Sidi Okba, Algeria. *Int. Rev. Spat. Plan. Sustain. Dev.* **2019**, *7*, 117–133. [[CrossRef](#)]
29. Coté, M. *La Ville et le Désert: Le Bas-Sahara Algérien*; Karthala: Paris, France, 2005.
30. Côte, M. *Signatures Sahariennes: Terroirs & Territoires vus du Ciel*; Presses Universitaires de Provence (PUP): Aix-en Provence, France, 2012.
31. Matallah, M.E.; Arrar, H.F.; Faci, M.; Mahar, W.A.; Ben Ratmia, F.Z.; Attia, S. Assessment of Human Outdoor Thermal Comfort in a Palm Grove during the Date Palm Phenological Cycle. *Atmosphere* **2022**, *13*, 379. [[CrossRef](#)]

32. Born Bouzaher, S.L.; Alkama, D. The requalification of the palm trees of Ziban as a tool for sustainable planning. *Procedia-Soc. Behav. Sci.* **2013**, *102*, 508–519. [[CrossRef](#)]
33. Center for the Built Environment (CBE). Available online: <https://clima.cbe.berkeley.edu/> (accessed on 1 August 2023).
34. Farhi, A. Biskra: De l'oasis à la ville saharienne (Note). *Méditerranée* **2002**, *99*, 77–82. [[CrossRef](#)]
35. Semahi, S.; Zemmouri, N.; Singh, M.K.; Attia, S. Comparative bioclimatic approach for comfort and passive heating and cooling strategies in Algeria. *Build. Environ.* **2019**, *161*, 106271. [[CrossRef](#)]
36. Haoui, S.; Chergui, S. Terre, pierre et bois dans l'architecture vernaculaire des Aurès et des Ziban: Des matériaux à usage complémentaire. *J. Mater. Environ. Sci.* **2016**, *7*, 3522–3531.
37. Harrison, G. *Meteorological Measurements and Instrumentation*; John Wiley & Sons: Hoboken, NJ, USA, 2014.
38. Mahdavinejad, M.; Moradchelleh, A.; Dehghani, S.; Mirhosseini, S.M. The adoption of central courtyard as a traditional archetype in contemporary architecture of Iran. *World Appl. Sci. J.* **2013**, *21*, 802–811.
39. Ouali, K.; El Harrouni, K.; Abidi, M.L.; Diab, Y. Analysis of Open Urban Design as a tool for pedestrian thermal comfort enhancement in Moroccan climate. *J. Build. Eng.* **2020**, *28*, 101042. [[CrossRef](#)]
40. Tsoka, S.; Tsikaloudaki, A.; Theodosiou, T. Analyzing the ENVI-met microclimate model's performance and assessing cool materials and urban vegetation applications—A review. *Sustain. Cities Soc.* **2018**, *43*, 55–76. [[CrossRef](#)]
41. Cohen, P.; Shashua-Bar, L.; Keller, R.; Gil-Ad, R.; Yaakov, Y.; Lukyanov, V.; Bar, P.; Tanny, J.; Cohen, S.; Potchter, O. Urban outdoor thermal perception in hot arid Beer Sheva, Israel: Methodological and gender aspects. *Build. Environ.* **2019**, *160*, 106169. [[CrossRef](#)]
42. Liu, Z.; Cheng, W.; Jim, C.Y.; Morakinyo, T.E.; Shi, Y.; Ng, E. Heat mitigation benefits of urban green and blue infrastructures: A systematic review of modeling techniques, validation and scenario simulation in ENVI-met V4. *Build. Environ.* **2021**, *200*, 107939. [[CrossRef](#)]
43. Rahul, A.; Edupuganti, S.R.; Naorem, V.; Mukherjee, M.; Brooks, T. Urban risk assessment tools and techniques for ecosystem-based solutions. In *Ecosystem-Based Disaster and Climate Resilience: Integration of Blue-Green Infrastructure in Sustainable Development*; Springer: Singapore, 2021; pp. 253–278.
44. Olesen, B.W.; Parsons, K.C. Introduction to thermal comfort standards and to the proposed new version of EN ISO 7730. *Energy Build.* **2002**, *34*, 537–548. [[CrossRef](#)]
45. Matallah, M.E.; Ahriz, A.; Zitouni, D.C.; Arrar, H.F.; Ratmia, M.A.E.B.; Attia, S. A methodological approach to evaluate the passive cooling effect of Oasis palm groves. *Sustain. Cities Soc.* **2023**, *99*, 104887. [[CrossRef](#)]
46. *ASHRAE Guideline 14-2002*; Measurement of Energy and Demand Savings. ASHRAE: Atlanta, GA, USA, 2002.

Disclaimer/Publisher's Note: The statements, opinions and data contained in all publications are solely those of the individual author(s) and contributor(s) and not of MDPI and/or the editor(s). MDPI and/or the editor(s) disclaim responsibility for any injury to people or property resulting from any ideas, methods, instructions or products referred to in the content.